Volume 9
Number 10
21 May 2021
Pages 3533-3886

Biomaterials Science

rsc.li/biomaterials-science

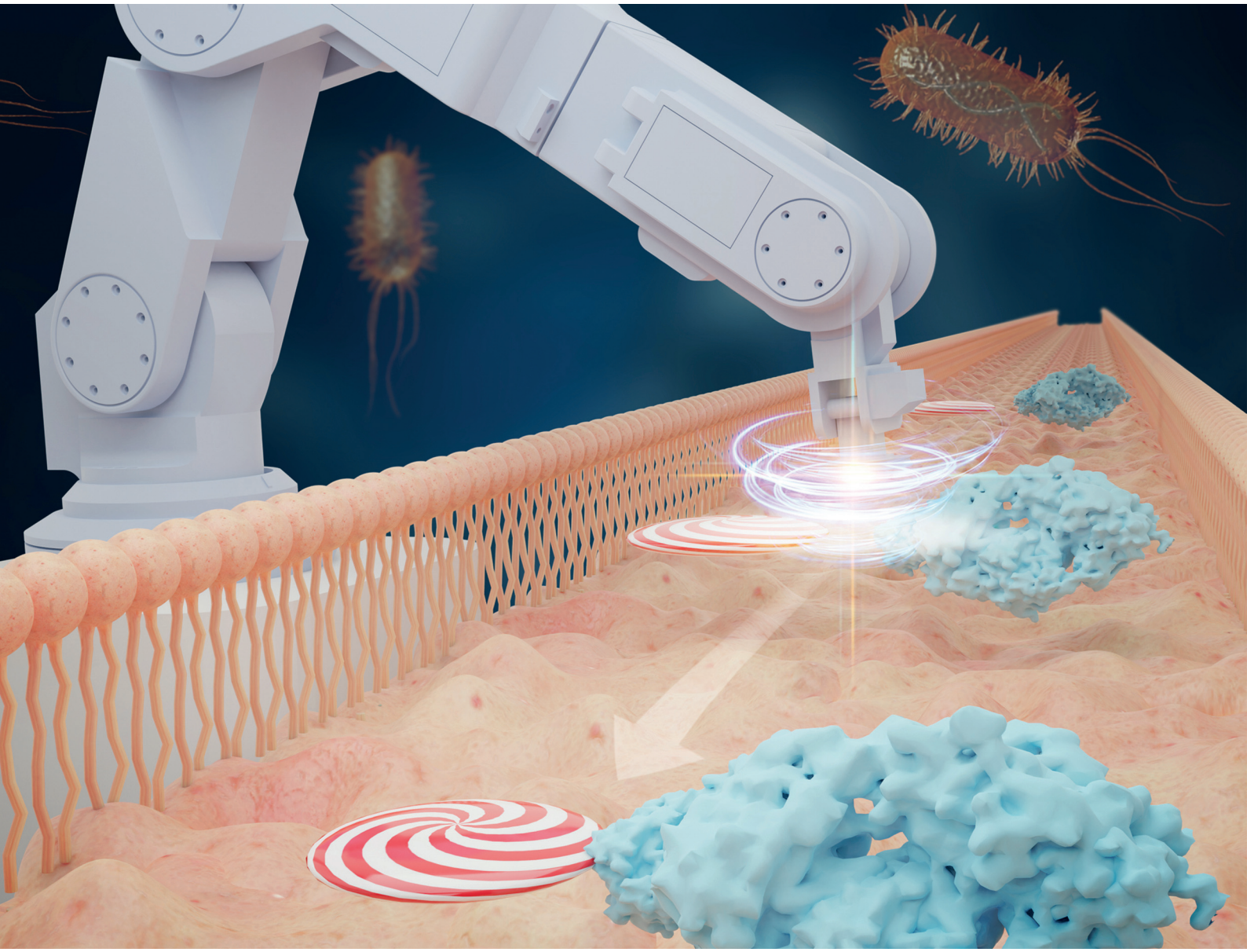

ISSN 2047-4849

ROYAL SOCIETY OF CHEMISTRY

PAPER
Urartu Ozgur Safak Seker *et al.*
Engineering of biofilms with a glycosylation circuit for biomaterial applications

European Society for Biomaterials

Biomaterials Science

ROYAL SOCIETY OF CHEMISTRY

PAPER

View Article Online
View Journal | View Issue

Cite this: *Biomater. Sci.*, 2021, **9**, 3650

Engineering of biofilms with a glycosylation circuit for biomaterial applications†

Ebru Sahin Kehribar, [a] Musa Efe Isilak,[a] Eray Ulas Bozkurt, [a] Jozef Adamcik,[b,c] Raffaele Mezzenga [b,c] and Urartu Ozgur Safak Seker *[a]

Received 25th December 2020,
Accepted 14th February 2021

DOI: 10.1039/d0bm02192j

rsc.li/biomaterials-science

Glycosylation is a crucial post-translational modification for a wide range of functionalities. Adhesive protein-based biomaterials in nature rely on heavily glycosylated proteins such as spider silk and mussel adhesive proteins. Engineering protein-based biomaterials genetically enables desired functions and characteristics. Additionally, utilization of glycosylation for biomaterial engineering can expand possibilities by including saccharides to the inventory of building blocks. Here, *de novo* glycosylation of *Bacillus subtilis* amyloid-like biofilm protein TasA using a *Campylobacter jejuni* glycosylation circuit is proposed to be a novel biomaterial engineering method for increasing adhesiveness of TasA fibrils. A *C. jejuni* glycosylation motif is genetically incorporated to *tasA* gene and expressed in *Escherichia coli* containing the *C. jejuni pgl* protein glycosylation pathway. Glycosylated TasA fibrils indicate enhanced adsorption on the gold surface without disruption of fibril formation. Our findings suggest that N-linked glycosylation can be a promising tool for engineering protein-based biomaterials specifically regarding adhesion.

1. Introduction

Protein glycosylation is a common form of post-translational modification in all domains of life. Glycosylation is critical for adhesiveness of proteins, and many adhesive proteins such as spider silk are heavily glycosylated.[1] Glycosylation in prokaryotes is generally associated with but not restricted to pathogenicity, due to increased adhesiveness to host cells.[2] Glycans can be covalently attached to the amide nitrogen of Asn (N-linked glycosylation) or hydroxyl oxygen of Ser and Thr (O-linked glycosylation).[3] *Campylobacter jejuni* is the first bacteria discovered with N-linked glycosylation. The *C. jejuni* glycosylation pathway became the most extensively studied bacterial glycosylation mechanism due to the transfer of the protein glycosylation (*pgl*) operon into *Escherichia coli.*[4] *pgl* is a 17 kb long operon with 12 genes. Glycan molecules are synthesized in the cytoplasm with the cooperative action of many enzymes and flipped to the periplasm by PglK flippase. In the periplasm, PglB oligosaccharyltransferase (OST) transfers the glycan *en bloc* on the nitrogen of Asn in the available D/E-X1-N-X2-S/T motif (X1 and X2 can be any amino acid except proline) and finalizes the glycosylation process.[5]

Biofilms are multicellular assemblies formed by many bacterial species in nature to help them tolerate harsh environmental conditions and mediate substrate adhesion. Bacteria in biofilms secrete a cohesive and protective extracellular matrix composed of nucleic acids, polysaccharides, other biomolecules, and protein fibers as scaffolds.[6] Amyloid and amyloid-like fibrils serve several functions in biofilms, especially during adhesion onto different surfaces and host cells.[7]

Amyloid biofilms are emerging functional biomaterials with broad applications. Recent efforts exploited the functionalization of amyloid fibrils for applications such as waste-water treatment, material synthesis, enzyme immobilization, and biomineralization due to their exquisite mechanical properties and ease of manipulation *via* genetic engineering.[8] As an example, a low complexity domain of FUS protein, a protein with slow amyloid formation kinetics, was constructed to have different functionalities to achieve multiblock, self-sorted supramolecular fibers.[9] Furthermore, curli fibrils fused with mussel foot proteins (Mfps) are reported as strong underwater adhesives.[10] Additionally, CsgA was fused with a chitin binding domain (CBD) and Mfps to create designer amyloid proteins and these fusions resulted in higher chitin binding activity.[11] Since *Bacillus subtilis* is generally regarded as safe (GRAS), its amyloid-like protein TasA is also used to create living materials with desired functionalities.[12] *B. subtilis* is

[a]*UNAM-Institute of Materials Science and Nanotechnology, Bilkent University, 06800 Ankara, Turkey. E-mail: urartu@bilkent.edu.tr*
[b]*ETH Zurich, Department of Health Sciences and Technology, 8092 Zurich, Switzerland*
[c]*Department of Materials, ETH Zurich, 8093 Zurich, Switzerland*

†Electronic supplementary information (ESI) available. See DOI: 10.1039/d0bm02192j

also utilized as cellular glues with tunable adhesive properties by fusing TasA with Mefp and BslA with mussel derived peptide Mfp3Sp.[13]

Until now, several functional groups have been attached to proteins to incorporate desired modifications and functions.[14] N-Linked glycosylation enabled a new ingredient in biomaterial design facilitating more ways to engineer organisms and molecules by including saccharides to the repertoire of building blocks. Most adhesive proteins being heavily glycosylated can imply many opportunities for glycosylation in protein-based biomaterial applications. Since biofilm proteins form adhesive fibrils with structural rigidity and robustness, *de novo* glycosylation may increase their adhesiveness.[15] Given the fact that amyloid-like TasA fibrils are utilized in biomaterial research, glycosylation appears to be a practical tool to alter adhesive properties. Consequently, the feasibility of TasA protein fibrils as adhesive materials may rise in several areas. In this work, we introduce and characterize glycosylation on TasA fibrils in terms of fibril structure, binding kinetics and adhesive properties. We engineered TasA protein to include the D/E-X1-N-X2-S/T (DQNAT) glycosylation motif at the C terminal and expressed it in *E. coli* containing the *pgl* circuit. Even though X1 and X2 can be any amino acid except proline, the DQNAT motif is the optimal site for glycosylation with PglB enzyme and the DQNAT motif is shown to be glycosylated in *E. coli* containing the *pgl* locus.[16] Subsequently, we matured the fibrils by incubating them at room temperature for different times (1 day, 7 days, 14 days and 28 days) and then, we examined the effect of N-linked glycosylation on fibril formation and viscoelastic properties of fibrils, as well as the time-dependent binding kinetics of TasA fibrils matured for different times on solid surfaces. To our knowledge, this is the first study that depicts successful glycosylation of an amyloid-like protein and analyzes the effects of glycosylation on fibril characteristics. We demonstrated that glycosylation could enhance adhesive properties of amyloid-like fibrils without disrupting fibrillization to produce biomaterials with superior adhesive performance.

2. Results

2.1. Genetic designs and glycosylation of TasA

In this study, we focused on TasA amyloid-like protein due to its functionalization capacity with peptide/protein inserts without losing its self-assembling properties, therefore allowing production of nanofibrils with additional desired functions.[11] Even though amyloid and amyloid-like proteins of biofilms were functionalized with several peptide/protein groups previously, their recombinant glycosylation has not been reported before. We examined the effect of glycosylation on adhesive and viscoelastic properties of purified TasA fibril. Firstly, we purified TasA and TasA-DQNAT proteins from *E. coli* without the *pgl* pathway as non-glycosylated proteins. TasA-DQNAT protein was also purified from *E. coli* with the *pgl* pathway as glycosylated protein. Purified proteins are matured to induce fiber formation by incubation at room temperature for different durations (Fig. 1a). For examining the effect of glycosylation on adhesive and viscoelastic properties, we first tested successful glycosylation of TasA. In the *pgl* pathway, transfer of glycans to DQNAT motif takes place in periplasmic space; therefore a pelB periplasmic localization signal is attached to the N-terminal of the *tasA*-DQNAT construct. Expression of the variants is confirmed by western blotting with anti-6X His antibody (Fig. 1b). Theoretical molecular weights of TasA and TasA-DQNAT (TasA D) proteins calculated using the Swissprot Expasy tool are ~27 kDa and ~28 kDa, respectively. In western blotting, the bands appear at ~35 kDa. There are additional bands at ~20 kDa and ~15 kDa. Those bands containing the poly-histidine tag are believed to correspond to the molecular weight of translated peptides from in-frame AUG codons in *tasA* gene or possible degradation products. Following, we investigated the glycosylation status of TasA D with the *pgl* pathway using soybean agglutinin (SBA) lectin blot. Lectins are proteins with affinity to specific sugar moieties and used instead of antibodies in lectin blot to detect protein glycosylation. SBA is a lectin with an affinity to terminal GalNAc of *C. jejuni* glycan.[17] Glycosylated TasA (TasA DP) is detected at ~35 kDa, ~20 kDa and ~15 kDa only in the DQNAT motif containing *tasA* and *pgl* pathway co-transformed samples, in correlation with the western blotting, indicating the successful glycosylation of TasA D protein and in frame peptides in the periplasmic space by the *pgl* pathway. Proteins further purified by size exclusion chromatography displayed single bands at ~35 kDa for both western and SBA blot (Fig. 1b).

2.2. Effect of glycosylation on the secondary structure

In order to observe the effects of DQNAT motif addition and glycosylation on the structure of TasA fibrils, we first analyzed changes in the secondary structures of 14 days old fibrils using circular dichroism (CD) (Fig. 2a). CD spectra of TasA displayed a minimum ~200 nm, a shoulder ~220 nm and a maximum ~190 nm, which is in correlation with the previously reported CD analysis of TasA oligomers and purified TasA fibrils.[18] TasA samples lack a high beta-sheet content which is typical of amyloid-like fibrils represented by a single minimum ~216 nm and a maximum ~197 nm; however a decrease in ellipticity in the range of 220–200 nm and an increase ~190 nm suggest the presence of beta-sheets in TasA fibrils. Additionally, two minima ~220 and ~200 nm indicate alpha helical characteristics. 14 days old TasA, TasA D and TasA DP display very similar CD spectra, indicating that addition of DQNAT motif or glycan groups did not alter the secondary structure significantly (Fig. 2a). In order to quantify structural elements, secondary structures were determined from CD data using the BestSel online tool.[19] Expectedly, BestSel calculations also revealed no significant change in the percentage of β-sheets or α-helices (Fig. 2b). CD spectrum and Bestsel secondary structure calculations of 1 day old, 7 day old and 28 day old TasA fibrils depicted similar structural behavior in response to the DQNAT motif and glycan addition, indicating that the maturation duration has no effect on the structural behavior of TasA, TasA D and TasA DP samples (Fig. S1†).

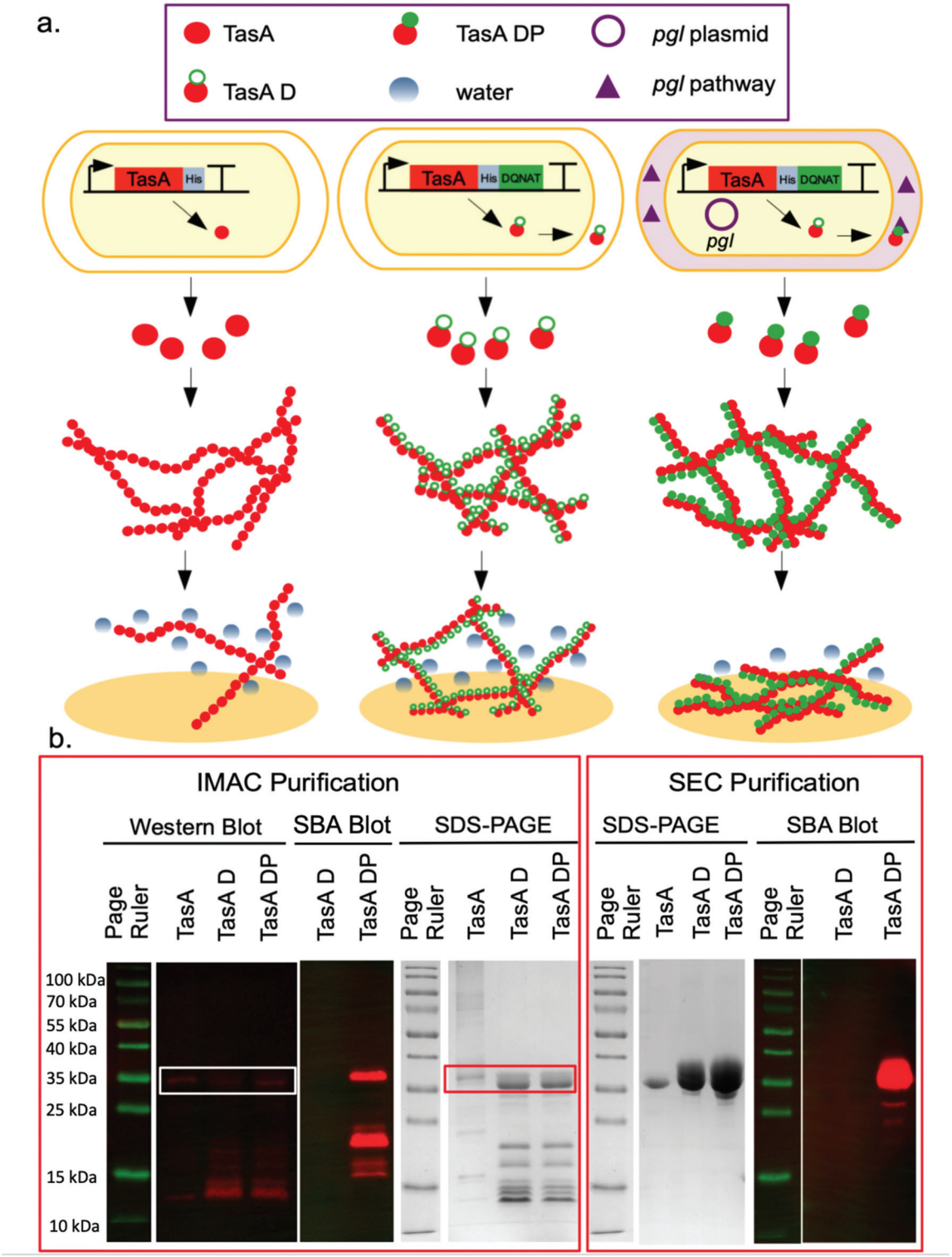

Fig. 1 a. A schematic representation of glycosylation effecting gold binding affinity and viscoelastic properties of TasA fibrils. b. Western blotting, SBA blotting and SDS-PAGE of affinity chromatography purified and SEC purified TasA, TasA D and TasA DP samples.

2.3. Analysis of fibrillization and fibril morphology

Despite the fact that CD analysis indicated no significant effect of glycosylation on the secondary structure, fibril formation or morphology could still be disrupted by the DQNAT motif or glycan groups. We examined matured samples with scanning transmission electron microscopy (STEM). STEM images of 14 day old samples revealed that the surfaces are

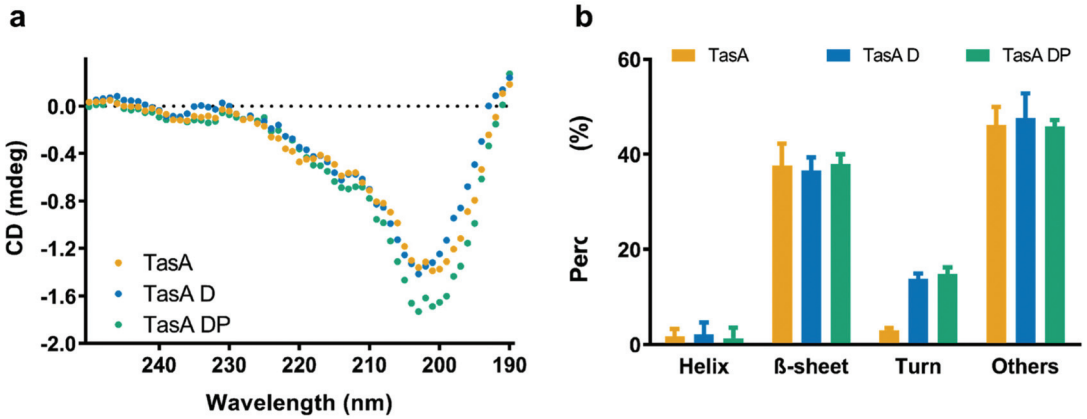

Fig. 2 a. Circular dichroism spectra of 14 days old TasA (orange dots), TasA D (blue dots) and TasA DP (green dots) samples. b. Percentages of secondary structures calculated by the BestSel online tool for 14 days old TasA (orange bars), TasA D (blue bars) and TasA DP (green bars) samples.

coated with wide film-like agglomerations and smaller aggregates (Fig. 3a) and upon DQNAT motif or glycan addition, film-like coatings are not disrupted. STEM images of 1 day, 7 day and 28 day old samples revealed similar structures (Fig. S2†). For analysis of smaller structures with better resolution, we characterized the 21 and 28 days old fibrils by atomic force microscopy (AFM). 3D AFM images of 28 days old TasA, TasA D and TasA DP samples exhibited small fibrillary structures (Fig. 3b). The height and length distribution of those fibril-like structures are analyzed with open source software FiberApp[20] (Fig. 3c) and the similarity of distributions is tested using Kolmogorov–Smirnov statistic. p values are greater than 0.05, therefore the distributions did not change significantly upon glycosylation. The average height is around 3 nm for all types of fibrils. The average length of formed fibrils where TasA fibrils are shortest while TasA DP fibrils are the longest; however the difference was not significant. Similarly, for the 21 day old sample, the same pattern in the fibril height and contour length is observed (Fig. S3†). The analysis depicted that the DQNAT motif or glycans did not significantly affect structures of small fibrils.

2.4. Analysis of adsorption kinetics and viscoelastic properties

Proteins, in general, tend to adhere more effectively on hydrophobic surfaces.[21] Glycoproteins, on the other hand, extensively adsorb on hydrophilic surfaces since the hydrophobic domains are masked by hydrophilic glycan groups.[22] Therefore, glycosylation of TasA could enhance its adsorption on hydrophilic surfaces. Since gold surfaces are used for several biomedical applications due to their biocompatibility and ease of functionalization, we analyzed the adsorption kinetics of matured TasA fibrils on gold surfaces with Quartz Crystal Microbalance with Dissipation (QCM-D) to assess the applicability of TasA protein as the surface coating material.[23] QCM-D records the frequency and dissipation change of a quartz crystal as a function of mass deposited on the surface at all the harmonics (n = 1,3,5,...,13), and provides real-time quantitative monitoring of surface-protein interactions as well as the viscoelastic properties of the deposited film.[24] Fig. 4a shows frequency shifts upon adsorption of 14 days old TasA, TasA D and TasA DP samples on gold QCM-D chips. Interaction of 1 μM samples resulted in a rapid initial decrease in the frequency, indicating the deposition of proteins on the sensor surface. Sequential administration of samples with increased concentrations (2 μM, 5 μM and 10 μM) caused further but slower drops in the frequency, as the surface coverage approaches saturation. Small changes in frequency were recorded upon rinsing, indicating that some of the adsorption was reversible in the studied time-scale. Applied protein concentration to the sensor surface correlates with resonance frequency shifts (Fig. 4b). This correlation indicates the strength of binding. Frequency shifts upon adsorption and their correlation with protein concentration for 1 day, 7 day and 28 day old samples are depicted in Fig. S4.†

Data collected from QCM-D experiments are used to calculate the desorption constant (k_d) of matured TasA, TasA D and TasA DP samples using eqn (1) (Table S3†), as reported in the literature before.[25] The least squares curve fitting was used to fit the simple adsorption model to experimental data in Fig. 4b to calculate f_{max} and k_d. Calculated desorption constants of 14 day old samples are demonstrated in Fig. 4c. DQNAT motif addition (TasA D) readily caused a significant ($p \leq 0.01$) decrease in k_d values compared to TasA samples. Furthermore, glycosylation (TasA DP) resulted in a more significant ($p \leq 0.0001$) decrease in k_d values, compared to TasA D samples. k_d calculations of 1 day, 7 day and 28 day old samples also displayed the same behavioral pattern (Fig. S5†), indicating that maturation durations did not alter the effect of glycosylation on adsorption kinetics. In addition, Gibbs free energy ($\Delta G°$) of adsorption is calculated for matured samples using eqn (2) (Table S4†). Correspondingly, $\Delta G°$ calculations revealed that TasA DP has significantly lower $\Delta G°$, implying that the adsorption of TasA DP onto the gold surface is thermodynamically more favorable and more stable, compared to TasA and TasA D for 14 day old samples (Fig. 4d). $\Delta G°$ calcu-

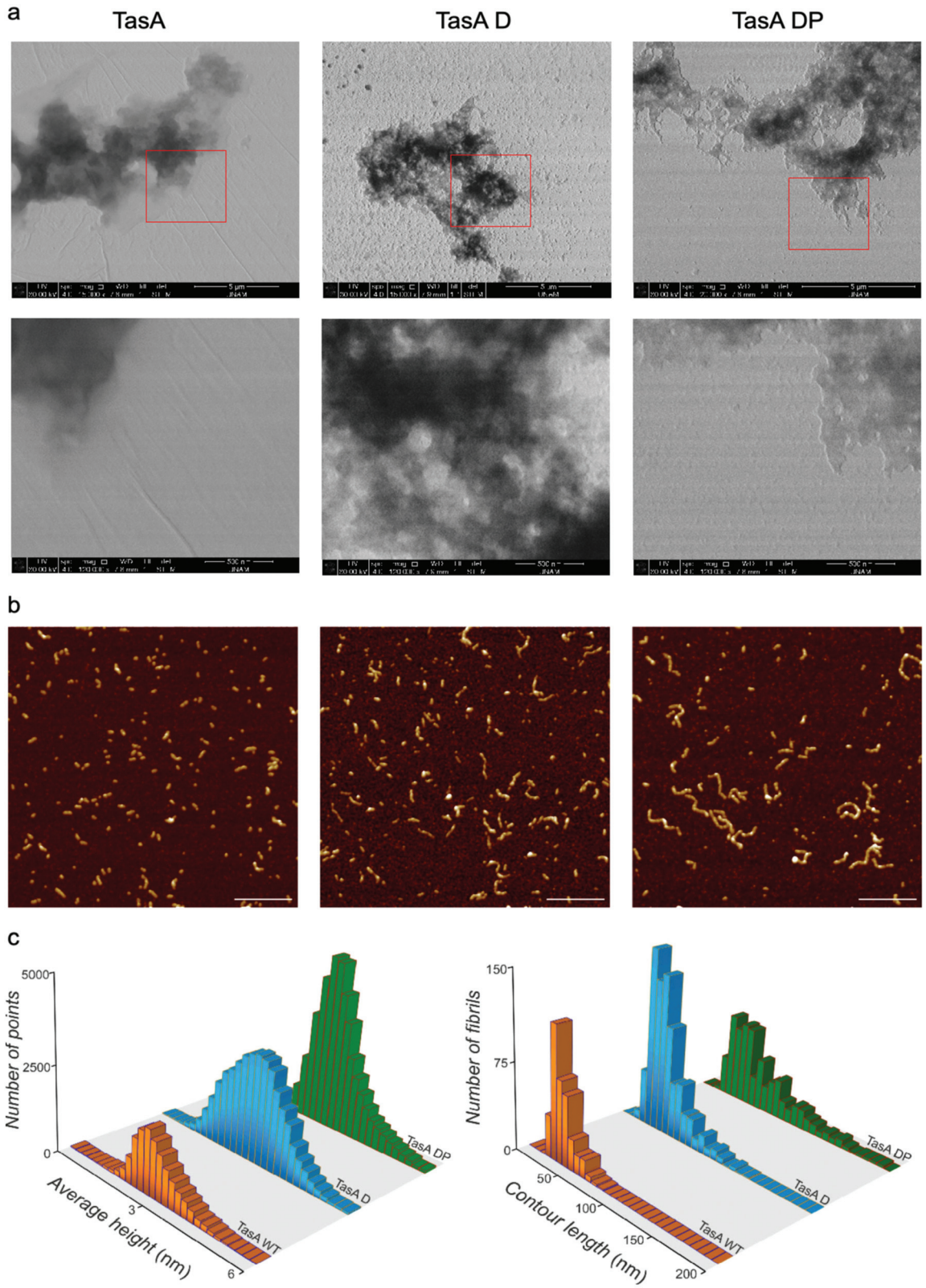

Fig. 3 Morphological characterization of 14 days old TasA, TasA D and TasA DP fibrils using a. Scanning transmission electron microscopy (STEM). Upper images are higher magnification versions of the areas in red boxes from lower images. b. Atomic force microscopy (AFM). Scale bar: 200 nm. c. AFM images analyzed with FiberApp software for quantification of the average fibril height and length.

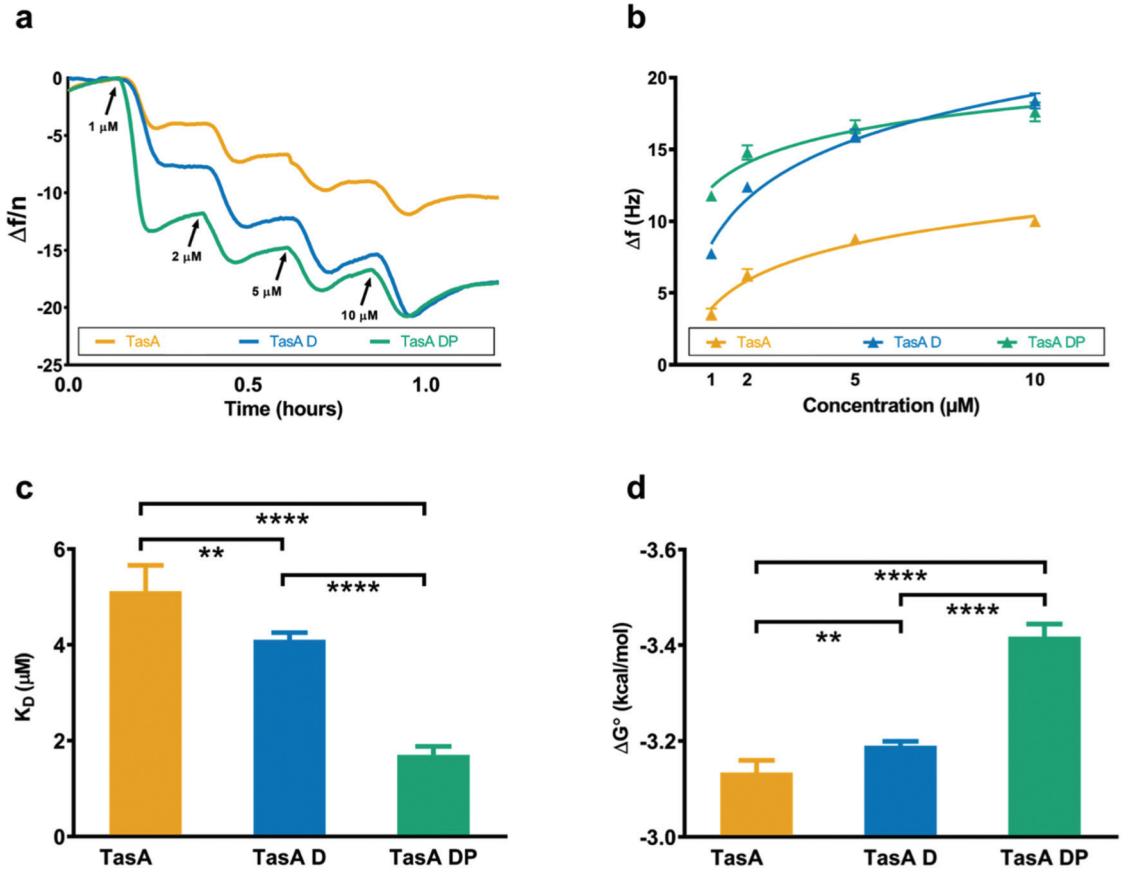

Fig. 4 a. The recorded frequency shifts in QCM-D upon adsorption with increasing concentrations b. Frequency shifts with respect to applied protein concentrations c. Calculated desorption constants (k_d) and *d*. Calculated Gibbs free energy (ΔG°) of 14 days old TasA, TasA-D and TasA-DP proteins. Significance values are calculated by the *t*-test, $n = 3$.

lations of 1 day, 7 day and 28 day samples also displayed the same behavioral pattern (Fig. S5†).

The frequency and dissipation change recorded with QCM-D measurements holds information about the amount of deposited mass and viscoelastic properties of deposited films, in addition to binding kinetics.[26] Proteins adsorbed on the QCM chip surface can be quantified with Δf; however protein layers have structural flexibility and viscoelasticity, which requires frequency and dissipation determination. The change of dissipation (ΔD) over the course of time is depicted in Fig. 5a for 14 day old TasA, TasA D and TasA DP samples on gold chips. Negative Δf (Fig. 4a) and positive ΔD (Fig. 5a) are characteristic of mass deposition, in our case protein adsorption. The decrease in dissipation during washing steps indicates that a fraction of adsorption is reversible. Dissipation changes over time for 1 day, 7 day and 28 day old samples are depicted in Fig. S6† and display a similar behavior.

QCM-D measures the mass of both protein and coupled water. Mass of the trapped, intra-layer or hydrodynamically coupled water also affects the viscoelastic response of the adsorbed layer.[27] An increase in dissipation corresponds to enhanced viscous behavior and conversely, a decrease in dissipation corresponds to enhanced elasticity.[27] Therefore, the $\Delta D/\Delta f$ ratio can be used to determine the flexibility of the deposited film, where a larger $\Delta D/\Delta f$ ratio is indicative of more viscous and flexible films.[28] Glycan groups are reported to structure water molecules in their vicinity and even in longer ranges; therefore glycosylated TasA samples are expected to represent a more viscous behavior.[29] Viscosity can enhance cell adhesion on surfaces and the viscoelastic properties of coating materials influence cellular behavior.[30] Therefore, characterization of viscoelastic properties can hold important clues in terms of designing functional surfaces. In order to understand the differences between viscoelastic properties of deposited films, we assessed $\Delta D/\Delta f$ ratios of TasA, TasA D and TasA DP samples with different maturation times (Fig. 5b). $\Delta D/\Delta f$ ratios are calculated from the end point of ΔD and Δf values after protein addition at different concentrations. Addition of the DQNAT motif significantly affects the $\Delta D/\Delta f$ ratio for 1 day old and 7 day old samples. At day 1, TasA has a higher ratio and at day 7, TasA D has a significantly higher ratio than TasA. However, for day 14 and 28, no significant difference is observed between $\Delta D/\Delta f$ ratios of TasA and TasA D samples. For all maturation times (1 day, 7 days, 14 days and 28 days), TasA DP has the lowest $\Delta D/\Delta f$ ratio. The $\Delta D/\Delta f$ ratio of the TasA sample was significantly higher than TasA DP at

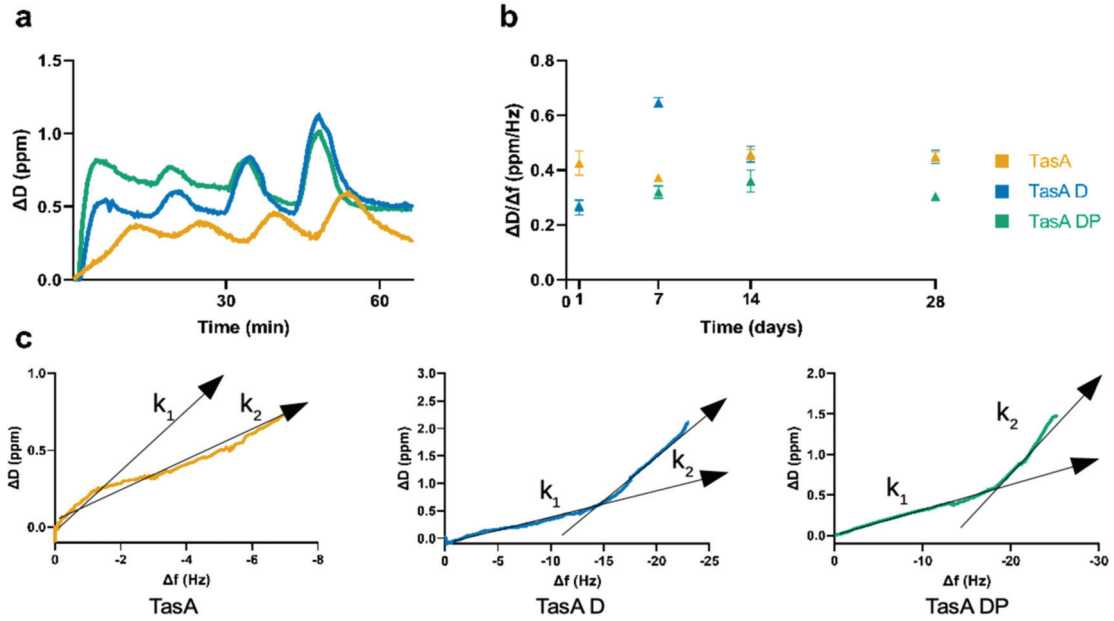

Fig. 5 a. The recorded dissipation shifts in QCM-D upon adsorption with increasing concentrations of 14 days old TasA, TasA-D and TasA-DP proteins b. Total $\Delta D/\Delta f$ ratios of matured TasA, TasA-D and TasA-DP fibrils. Significance values are calculated by the *t*-test, $n = 3$. c. ΔD *vs.* Δf plots of 14 days old TasA, TasA D and TasA DP proteins, with corresponding color codes.

all time points. For day 1, TasA D and Tasa DP have no significant difference in terms of $\Delta D/\Delta f$ ratio, however as the maturation duration increased, the $\Delta D/\Delta f$ ratio of TasA D was significantly higher than that of TasA DP.

The $\Delta D/\Delta f$ ratio does not only vary between samples, but also varies with maturation time (Fig. 5b). The viscoelastic behavior of different samples over the time shows some discrepancies. For TasA, the $\Delta D/\Delta f$ ratio does not change significantly in day 7, increases significantly ($p < 0.01$) at day 14 and then does not display any further significant change. Overall, the $\Delta D/\Delta f$ ratio of TasA fibrils is not affected by maturation from day 1 to day 28. For TasA D, the $\Delta D/\Delta f$ ratio increases significantly in day 7 ($p < 0.0001$) unlike TasA, but shows a sharp decrease at day 14 ($p < 0.001$) and then does not display any further significant change. However, between day 1 and day 28, the $\Delta D/\Delta f$ ratio of TasA D fibrils increased significantly ($p < 0.001$). TasA DP, on the other hand, shows an increase in the $\Delta D/\Delta f$ ratio at day 7 with respect to day 1 ($p < 0.05$), and then does not display any further significant change in day 14 and day 28. Overall, there is no significant change in 1 day old and 28 day old TasA DP fibrils in terms of $\Delta D/\Delta f$ ratio. Even though only TasA D samples demonstrated a significant change in viscoelastic properties between day 1 and day 28 samples, all samples displayed alterations at different time points during the maturation process. Overall, viscoelastic properties of TasA and TasA DP fibrils did not change significantly, whereas TasA D fibrils showed increased viscosity and flexibility over the course of time.

In order to understand the viscoelastic properties of deposited films over time with increasing concentration, we plotted ΔD *vs.* Δf graphs of TasA, TasA D and TasA DP samples with different maturation times. The plots for 14 day old samples are depicted in Fig. 5c. ΔD *vs.* Δf plots can reveal differences between adsorption behavior of proteins, not directly observed from time dependent ΔD or Δf plots. For all proteins, ΔD *vs.* Δf graphs display two different phases with different slopes along the adsorption process, indicated with black arrows. Those different slopes depicted as k_1 and k_2 indicate at least two different kinetic processes.[31] For TasA, the initial slope is much higher and the slope after the break point is lower than other proteins ($k_1 = 0.93$ and $k_2 = 0.41$). These data depict that a flexible layer is formed initially, and the flexibility of the layer is decreased with increasing protein concentration. For TasA D and TasA DP samples, the initial slope k_1 and the slope after the break point k_2 are very similar (k_1 TasA $D = 0.25$ and k_1 TasA DP $= 0.27$, k_2 TasA $D = 0.92$ and k_2 TasA DP $= 1$) indicating a similar adsorption kinetics for glycosylated and non-glycosylated samples. In contrast to TasA, larger k_2 values indicate a rigid initial layer and increased flexibility with increasing protein concentration. The biphasic adsorption kinetics indicates an initial adsorption onto surfaces, followed by the rearrangements/conformational changes within the adsorbed layer.[31] As explained previously, proteins separated on the surface result in higher dissipation at low surface coverages. The higher k_1 value of TasA can arise from lower surface coverage at low protein concentrations, in correlation with its higher k_d value. As the surface coverage increases with high protein concentrations, close packing results in more rigid films and less dissipation.

2.5. Effect of glycosylation on cell adhesion

Understanding cell adhesion behavior on a surface is of crucial importance for biomaterial studies, as desired cell

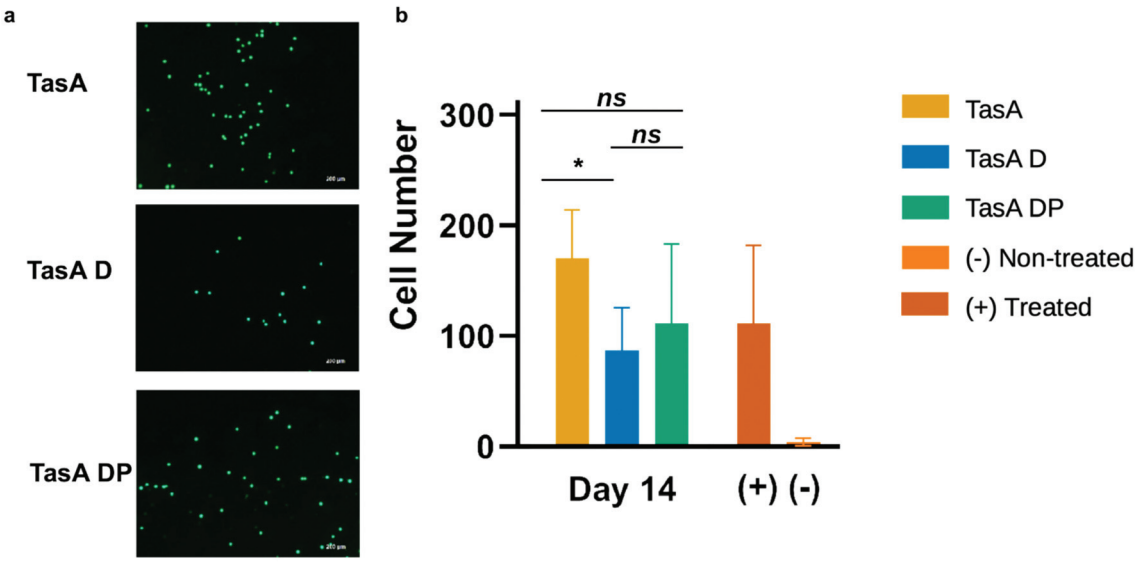

Fig. 6 Adhesion of HEK293 cells on surfaces coated with 14 days old TasA, TasA D and TasA DP. a. Representative images of Calcein AM labelled adhered cells and b. Quantitative analysis of adhered number of cells, n = 3.

adhesion properties may be different for each application. For example, biomaterials that interact with blood such as artificial vessels are required to be non-adherent to cells, whereas scaffolds for tissue generation studies need to promote cell adhesion to the material.[32] Thus, we determined the cell adhesion capacity for matured TasA, TasA D and TasA DP fibrils using HeLa S3 cells to analyze the effect of maturation and glycosylation on cell adhesive properties. Representative fluorescence microscopy images of Calcein AM labeled adhered cells are depicted in Fig. 6a and the total number of adhered cells is summarized in Fig. 6b. Even though the number of adhered cells appears to decrease by DQNAT motif addition and increase by glycan addition, the high variation between each experimental set leads to an insignificant change in cell adhesion capacity of glycosylated samples. However, glycosylated or non-glycosylated, all samples have cell adhesion capacity in the range of positive control. These data suggest that glycosylated TasA fibrils possess improved affinity to gold surfaces and can be utilized in applications that require cellular adhesion.

3. Conclusion

Biofilms are widely utilized adhesive materials composed of both living and nonliving components. In nature, these self-assembling multilayer structures protect bacteria from challenging environments and are often linked to pathogenicity due to enhanced adhesiveness to host cells. Its adhesiveness, along with many other properties, has been utilized in many applications. When other adhesive proteins in nature are envisioned, such as silk and mussel foot proteins (Mfps), they are found highly glycosylated. Here, we combined two pro-adhesiveness components, *B. subtilis* biofilm protein TasA and *C. jejuni* glycosylation pathway and successfully produced recombinant glycosylated TasA proteins as a novel method to enhance adhesive properties. We calculated the desorption constant (k_d) and Gibbs free energy ($\Delta G°$) of adsorption and found that TasA DP has lower k_d and $\Delta G°$, suggesting that glycosylation significantly improved adsorption characteristics of TasA to the gold surface. This enhancement in the surface adsorption can be due to the interaction of hydrophilic glycan groups on the surface of the proteins with oxidized gold surface. This can also explain the enhanced adsorption upon addition of a hydrophilic DQNAT motif. CD, STEM and AFM data suggested that glycosylation of biofilm proteins did not affect the secondary structure. Even though the contour length of the fibrils has changed upon DQNAT motif or glycan addition, the height of the fibrils remains unchanged and film-like coatings are not disrupted.

We also investigated viscoelastic properties of TasA, TasA D and TasA DP by analyzing $\Delta D/\Delta f$ plots and observed that glycosylated TasA forms a more compact and rigid layer, compared to TasA and TasA D. Normally, glycan groups are known to interact with water molecules, therefore, expected to increase hydration and viscosity. However, the amount of coupled water is also related to how protein packs within the interface.[26] If the interaction of the protein with the surface is stronger than the interaction within the protein, proteins can form a closely packed, rigid thin layer on the surface resulting in higher surface coverage, therefore, entrapping less water within the film. In addition, this could result in reduced film flexibility due to electrostatic repulsion between the densely packed groups.[26] Noting that glycosylated samples result in high affinity to the gold surface, lower dissipation values of glycosylated samples suggest the formation of a denser thin layer and

higher surface coverage due to increased surface affinity (Fig. 1a). Glycosylation of the DQNAT motif in TasA resulted in lower dissipation values, which indicated higher surface coverage that results in less water entrapment and reduced flexibility. In addition, charge of glycans may also contribute to the reduced flexibility of densely packed films, due to electrostatic repulsion.

Conformational rearrangements during the maturation process can alter secondary structures. When $\Delta D/\Delta f$ plots and secondary structure predictions are co-analyzed, a significant increase in the $\Delta D/\Delta f$ ratio is observed (Fig. 6b) between day 7 and day 14, which is in correlation with a significant increase in anti-parallel beta sheets and a significant decrease in alpha helical structures. On day 28, the percentage of anti-parallel beta sheets decreases significantly and displays no significant difference between day 1 and day 28. TasA D has an increased $\Delta D/\Delta f$ ratio between day 1 and day 7 and a significant increase in anti-parallel beta sheets, similar to TasA. A decreased $\Delta D/\Delta f$ ratio is accompanied by a decrease in the alpha helical structure between day 7 and day 14, while the anti-parallel beta sheet content remains the same. Between day 1 and day 28, no significant change is observed in the percentage of secondary structures; however the $\Delta D/\Delta f$ ratio is significantly increased. For TasA DP, alpha helix and beta sheet content of the sample is altered significantly between day 14 and day 28, however those changes are not detected as a change in $\Delta D/\Delta f$ ratio. Similarly, the small increase in the $\Delta D/\Delta f$ ratio between day 1 and day 7 is not detected as a significant change in secondary structures. These data suggest that the differences in viscoelastic properties are not solely due to structural rearrangements but also differences in hydration capacity contributions to viscous and elastic properties of the samples. Taken together, the fluctuation in percentages of secondary structure elements along with the associated water molecules can alter $\Delta D/\Delta f$ ratios.

Biocompatibility of a surface is generally related to cell adhesion onto the surface.[33] Glycosylated TasA fibrils with different maturation times are reported to support cell adhesion. In conclusion, glycosylated TasA fibrils hold potential as biocompatible coating or scaffold materials for applications that require enhanced cell adhesion such as tissue engineering, wound sealants and medical devices. Due to their higher adsorption affinity and higher surface coverage, glycosylated TasA fibrils may be utilized as superior coating materials.

4. Experimental section/methods

4.1. Genetic designs and clonings

The *tasA* gene was retrieved from the genome of wild-type *B. subtilis 168*. Cells were grown overnight, and genomic DNA was isolated according to the manufacturer's guidelines (QIAamp genomic DNA kit). Genomic DNA was amplified using Q5 DNA polymerase (New England Biolabs, M0941S) with primers targeting the *tasA* open reading frame (TasA-DQNAT-F and TasA-DQNAT-R). To create a pET-22b (+) plasmid with the *pgl* glycosylation recognition site after polyhistidine tag, the DQNAT motif was added to pET-22b (+) plasmid *via* PCR using forward primers with DQNAT motif in the overhang region (DQNAT_pet22b_F and DQNAT_pet22b_R). Primer sequences used for PCR reactions are listed in Table S1.† For TasA cloning, the resulting DNA fragments and the pET-22b (+) plasmid were restriction digested by high fidelity KpnI (New England Biolabs, R3142) and XhoI (New England Biolabs, R0146) enzymes to create sticky ends. For TasA-DQNAT cloning, tasA PCR fragments with suitable restriction sites and pet22b (+) PCR fragments with DQNAT were restriction digested by high fidelity SacI (New England Biolabs, R3156S) and AvrII (New England Biolabs, R0174S) enzymes to create sticky ends. DNA was ligated by T4 DNA ligase (New England Biolabs, M0202), using the manufacturer's protocol, then transformed a chemically competent strain of *E. coli* DH5α PRO by heat shock transformation. All incubations in this study were performed at 37 °C, 200 rpm. For all constructs, selected colonies were verified by Sanger sequencing (Genewiz, USA). The amino acid sequences of each design are listed in Table S2.†

4.2. Protein purification

To obtain proteins without glycosylation, *tasA* without DQNAT and *tasA*-DQNAT constructs were transformed to *E. coli BL21 (DE3)* strain. To obtain proteins with glycosylation, *tasA*-DQNAT construct was transformed to *E. coli BL21 (DE3)* strain containing the *pgl* pathway from *C. jejuni*, a generous gift from Markus Aebi. Cells were grown in the auto-induction medium for 24 hours at 37 °C, 200 rpm.[34] Cells are harvested by centrifugation and resuspended in 1× PBS containing guanidine hydrochloride (6 M), imidazole (20 mM) and Tween-20 (0.2%). The suspension was sonicated at 30% power for 3 minutes with 10 s on/20 s off cycles. Samples were centrifuged at 21.500*g* for 1 hour and the supernatant was filtered with a 0.45 μm filter. Filtered lysate was loaded on a pre-equilibrated HisTrap nickel column (GE life sciences 17524701) and washed 10 volumes of 1× PBS containing guanidine hydrochloride (6 M) and imidazole (20 mM). Finally, proteins were eluted with 5 volumes of 1× PBS containing guanidine hydrochloride (6 M) and imidazole (500 mM). To remove guanidine hydrochloride and induce fibrillization of proteins, samples were dialyzed against water for 2 hours at room temperature and then for O/N at +4 °C in fresh water, with gentle stirring.

4.3. SDS-PAGE, western blotting and SBA blotting

Samples were boiled at 95 °C for 1 hour with 1× SDS loading dye. Boiled samples were electrophoresed on 15% SDS-polyacrylamide gel. For Coomassie staining, the gel was placed into the Coomassie blue staining solution and heated in the microwave without boiling. After 1 hour of shaking in the dye solution, the gel was incubated in destaining solution (60% ddH_2O, 30% methanol, 10% acetic acid) until the bands were clearly visible. For western blotting, the gel was transferred to the PVDF membrane using Trans Blot Turbo (Biorad) following the manufacturer's instructions. The membrane was blocked

with 5% milk in TBS-T for 1 hour at room temperature with rocking. Then the membrane was placed in 5% milk in TBS-T containing 1 : 5000 primary anti-his mouse antibody (PTGLAB 66005) and incubated at 4 °C overnight with rocking. The membrane was washed in TBS-T with shaking, then incubated in 5% milk in TBS-T containing 1 : 5000 horseradish peroxidase (HRP) conjugated goat anti-mouse secondary antibody (Abcam ab6789-1 MG) for 1 hour at room temperature. After washing in TBS-T with shaking, the membrane was incubated in the ECL substrate (Biorad 170-5060) following the manufacturer's protocol and visualized using Chemidoc (Biorad) with appropriate settings. For soybean agglutinin (SBA) lectin blot, after transferring proteins to the PVDF membrane, the membrane was blocked with 5% bovine serum albumin (BSA) in TBS-T for 2 hours with rocking at room temperature. The membrane was transferred into 5% BSA in TBS-T containing 1 : 2500 HRP conjugated SBA (Sigma Aldrich, L1395) and incubated for 1 hour at room temperature with rocking. The membrane was washed with TBS-T with shaking and incubated in the ECL substrate following the manufacturer's protocol. The membrane was visualized using Chemidoc with appropriate settings.

4.4. Circular dichroism (CD)

The CD spectra of samples were measured from 300 nm to 190 nm with 5 repeats (Jasco J-815) at room temperature with 300 s delay time, 1 mm bandwidth. Data were analyzed using the Bestsel online tool for secondary structure analysis.[19]

4.5. Atomic force microscopy (AFM)

For formation of amyloid-like fibrils, following affinity chromatography, size exclusion chromatography was performed using HiPrep 16/60 Sephacryl S-200 HR SEC column (GE lifesciences) according to the manufacturer's protocol. 1× PBS containing guanidine hydrochloride (6 M) was used as the mobile phase. Then, proteins were desalted into NaCl (25 mM) using a HiTrap desalting column (GE lifesciences). Desalted proteins are incubated at room temperature over a period of 28 days. At day 21 and 28, samples were prepared for imaging. The protein sample (100 μl) was incubated for 3 minutes on a freshly cleaved mica surface. Treated mica was rinsed with ddH_2O, and then dried with nitrogen stream. The AFM was operated at tapping mode using silica cantilevers. The acquired images are used for height and length analysis of fibrils with the open source software FiberApp.[20] The fibril height and length distributions of TasA, TasA D and TasA DP were compared with each other using the Kolmogorov–Smirnov statistic test. p values were calculated, and distributions were accepted as the same if the p value is greater than 0.05.

4.6. Quartz crystal microbalance (QCM)

The QCM sensors were cleaned with basic piranha solution (1 : 3 Hydrogen peroxide : Ammonia) at 70 °C, washed in ddH_2O and dried with N_2 stream before measurements. The QCM sensor was equilibrated with the ddH_2O. Proteins were diluted to 1 μM, 2 μM, 5 μM and 10 μM samples and sonicated at sonic baths just before use. Samples with increasing concentrations were applied with a constant flow rate (30 μL per minute) for 3 minutes at 25 °C. Between each concentration, the QCM sensor was equilibrated with the ddH_2O for 10 minutes. F1, F3, F5, F7, F9, F11 and F13 harmonics were collected during the experiments on a QSense explorer QCM device with a gold coated sensor (Biolin Scientific).

To characterize the effect of glycosylation on the adsorption of TasA samples onto gold sensor surfaces, data from five different overtone orders were analyzed using the simple adsorption model.

$$\Delta f = (f_{\max} \times C)/(k_d + C) \quad (1)$$

where C was the protein concentration, the f_{max} value was estimated from the adsorption isotherm, and the k_d value was determined by least-squares fitting. ΔG° values were calculated according to

$$\Delta G^\circ = -RT\ln(k_{eq}) \quad (2)$$

where R was the ideal gas constant (1.987 kcal K^{-1} mol^{-1}), T was temperature at Kelvin scale, and k_{eq} was $1/k_d$. Statistical significance between experimental sets was calculated using Student's t-test.

4.7. Cell adhesion

Non-treated 96 well plates were coated with matured TasA, TasA D and TasA DP samples (10 μM). Samples (50 μl) were dried on the wells, as triplicate. The wells were blocked with 0.1% BSA in DMEM, and overnight at +4 °C. Next day, 5×10^4 HeLa S3 cells were added to each well in FBS free DMEM with 0.1% BSA and adhered for 90 minutes in the incubator. Following, non-adherent cells were washed with PBS three times and for recovery, adhered cells were incubated in 10% FBS DMEM for 4 hours in an incubator. Wells were washed with PBS 3 times and dyed with Calcein AM (1 μM) for 30 minutes. The adhered cells were visualized with an inverted fluorescent microscope and cells were counted from 3 different points for each well. Experiments are conducted in triplicate. Statistical significance between experimental sets was calculated using Student's t-test.

Conflicts of interest

The authors declare no conflict of interest.

Acknowledgements

The study was supported by TUBITAK Project 216M127. UOSS acknowledges the TUBA-GEBIP Award, TUSEB Aziz Sancar Award and Science Academy Award. The authors thank Markus Aebi for *pgl* pathway plasmid. We also thank Prof. Hilmi Volkan Demir for allowing us to use the Quartz Crystal Microbalance device.

UOSS conceived the idea. UOSS, ESK and MEI designed the circuits and the experimental plan. MEI carried out cloning, glycosylation assay and protein purifications. ESK conducted CD and STEM analysis. ESK and EUB run the QCM measurements together. RM and JA designed AFM experiments and JA run the AFM experiments and data analysis. ESK analyzed the QCM data and carried out cell adhesion experiments. All the authors contributed to the writing of the manuscript.

References

1 E. Hennebert, B. Maldonado, P. Ladurner, P. Flammang and R. Santos, *Interface Focus*, 2015, **5**, 20140064.
2 (*a*) F. Y. Y. Tan, C. M. Tang and R. M. Exley, *Trends Biochem. Sci.*, 2015, **40**, 342; (*b*) M. A. Schmidt, L. W. Riley and I. Benz, *Trends Microbiol.*, 2003, **11**, 554.
3 H. Nothaft and C. M. Szymanski, *Nat. Rev. Microbiol.*, 2010, **8**, 765.
4 (*a*) C. M. Szymanski, R. Yao, C. P. Ewing, T. J. Trust and P. Guerry, *Mol. Microbiol.*, 1999, **32**, 1022; (*b*) M. Wacker, *Science*, 2002, **298**, 1790.
5 (*a*) H. Li, A. W. Debowski, T. Liao, H. Tang, H.-O. Nilsson, B. J. Marshall, K. A. Stubbs and M. Benghezal, *Future Microbiol.*, 2017, **12**, 59; (*b*) D. Linton, N. Dorrell, P. G. Hitchen, S. Amber, A. V. Karlyshev, H. R. Morris, A. Dell, M. A. Valvano, M. Aebi and B. W. Wren, *Mol. Microbiol.*, 2005, **55**, 1695.
6 H.-C. Flemming and J. Wingender, *Nat. Rev. Microbiol.*, 2010, **8**, 623.
7 E. P. DeBenedictis, J. Liu and S. Keten, *Sci. Adv.*, 2016, **2**, e1600998.
8 (*a*) S. Bolisetty and R. Mezzenga, *Nat. Nanotechnol.*, 2016, **11**, 365–371; (*b*) P. Q. Nguyen, Z. Botyanszki, P. K. R. Tay and N. S. Joshi, *Nat. Commun.*, 2014, **5**, 4945; (*c*) E. Kalyoncu, R. E. Ahan, C. E. Ozcelik and U. O. S. Seker, *Adv. Mater.*, 2019, **31**, 1902888; (*d*) T. T. Olmez, E. Sahin Kehribar, M. E. Isilak, T. K. Lu and U. O. S. Seker, *ACS Synth. Biol.*, 2019, **8**, 2152; (*e*) R. E. Ahan, B. Saltepe, O. Apaydin and U. O. S. Seker, *ChemBioChem*, 2019, **20**, 1799–1809; (*f*) X. Yang, Z. Li, H. Xiao, N. Wang, Y. Li, X. Xu, Z. Chen, H. Tan and J. Li, *Adv. Funct. Mater.*, 2018, **28**, 1802730; (*g*) C. Li, A.-K. Born, T. Schweizer, M. Zenobi-Wong, M. Cerruti and R. Mezzenga, *Adv. Mater.*, 2014, **26**, 3207.
9 B. An, X. Wang, M. Cui, X. Gui, X. Mao, Y. Liu, K. Li, C. Chu, J. Pu, S. Ren, Y. Wang, G. Zhong, T. K. Lu, C. Liu and C. Zhong, *ACS Nano*, 2017, **11**, 6985.
10 C. Zhong, T. Gurry, A. A. Cheng, J. Downey, Z. Deng, C. M. Stultz and T. K. Lu, *Nat. Nanotechnol.*, 2014, **9**, 858.
11 M. Cui, Q. Qi, T. Gurry, T. Zhao, B. An, J. Pu, X. Gui, A. A. Cheng, S. Zhang, D. Xun, M. Becce, F. Briatico-Vangosa, C. Liu, T. K. Lu and C. Zhong, *Chem. Sci.*, 2019, **10**, 4004.
12 J. Huang, S. Liu, C. Zhang, X. Wang, J. Pu, F. Ba, S. Xue, H. Ye, T. Zhao, K. Li, Y. Wang, J. Zhang, L. Wang, C. Fan, T. K. Lu and C. Zhong, *Nat. Chem. Biol.*, 2019, **15**, 34.
13 C. Zhang, J. Huang, J. Zhang, S. Liu, M. Cui, B. An, X. Wang, J. Pu, T. Zhao, C. Fan, T. K. Lu and C. Zhong, *Mater. Today*, 2019, **28**, 40.
14 (*a*) T. T. Olmez, E. Sahin Kehribar, M. E. Isilak, T. K. Lu and U. O. S. Seker, *ACS Synth. Biol.*, 2019, **8**, 2152; (*b*) R. E. Ahan, B. Saltepe, O. Apaydin and U. O. S. Seker, *ChemBioChem*, 2019, **20**, 1799–1809; (*c*) X. Yang, Z. Li, H. Xiao, N. Wang, Y. Li, X. Xu, Z. Chen, H. Tan and J. Li, *Adv. Funct. Mater.*, 2018, **28**, 1802730; (*d*) C. Li, A.-K. Born, T. Schweizer, M. Zenobi-Wong, M. Cerruti and R. Mezzenga, *Adv. Mater.*, 2014, **26**, 3207; (*e*) C. Zhong, T. Gurry, A. A. Cheng, J. Downey, Z. Deng, C. M. Stultz and T. K. Lu, *Nat. Nanotechnol.*, 2014, **9**, 858; (*f*) C. Zhong, T. Gurry, A. A. Cheng, J. Downey, Z. Deng, C. M. Stultz and T. K. Lu, *Nat. Nanotechnol.*, 2014, **9**, 858.
15 E. Axpe, A. Duraj-Thatte, Y. Chang, D.-M. Kaimaki, A. Sanchez-Sanchez, H. B. Caliskan, N.-M. Dorval Courchesne and N. S. Joshi, *ACS Biomater. Sci. Eng.*, 2018, **4**, 2100.
16 M. M. Chen, K. J. Glover and B. Imperiali, *Biochemistry*, 2007, **46**, 5579.
17 J. Kelly, H. Jarrell, L. Millar, L. Tessier, L. M. Fiori, P. C. Lau, B. Allan and C. M. Szymanski, *J. Bacteriol.*, 2006, **188**, 2427.
18 (*a*) L. Chai, D. Romero, C. Kayatekin, B. Akabayov, H. Vlamakis, R. Losick and R. Kolter, *J. Biol. Chem.*, 2013, **288**, 17559; (*b*) D. Romero, C. Aguilar, R. Losick and R. Kolter, *Proc. Natl. Acad. Sci. U. S. A.*, 2010, **107**, 2230.
19 (*a*) A. Micsonai, F. Wien, É. Bulyáki, J. Kun, É. Moussong, Y.-H. Lee, Y. Goto, M. Réfrégiers and J. Kardos, *Nucleic Acids Res.*, 2018, **46**, W315; (*b*) A. Micsonai, F. Wien, L. Kernya, Y.-H. Lee, Y. Goto, M. Réfrégiers and J. Kardos, *Proc. Natl. Acad. Sci. U. S. A.*, 2015, **112**, E3095.
20 I. Usov and R. Mezzenga, *Macromolecules*, 2015, **48**, 1269.
21 G. Anand, S. Sharma, A. K. Dutta, S. K. Kumar and G. Belfort, *Langmuir*, 2010, **26**, 10803.
22 M. Rabe, D. Verdes and S. Seeger, *Adv. Colloid Interface Sci.*, 2011, **162**, 87.
23 N. Elahi, M. Kamali and M. H. Baghersad, *Talanta*, 2018, **184**, 537.
24 S. Huang, Q. Hou, D. Guo, H. Yang, T. Chen, F. Liu, G. Hu, M. Zhang, J. Zhang and J. Wang, *RSC Adv.*, 2017, **7**, 39530.
25 (*a*) T. Onur, E. Yuca, T. T. Olmez and U. O. S. Seker, *J. Colloid Interface Sci.*, 2018, **520**, 145; (*b*) T. T. Olmez, E. Yuca, E. Eyupoglu, H. B. Catalak, O. Sahin and U. O. S. Seker, *ACS Omega*, 2018, **3**, 585; (*c*) U. O. S. Seker, A. Y. Chen, R. J. Citorik and T. K. Lu, *ACS Synth. Biol.*, 2017, **6**, 266.
26 E. A. Vogler, *Biomaterials*, 2012, **33**, 1201.
27 J. R. Clegg, C. M. Ludolph and N. A. Peppas, *J. Appl. Polym. Sci.*, 2020, **137**, 48655.
28 K. M. M. Aung, X. Ho and X. Su, *Sens. Actuators, B*, 2008, **131**, 371.
29 R. M. Espinosa-Marzal, G. Fontani, F. B. Reusch, M. Roba, N. D. Spencer and R. Crockett, *Biophys. J.*, 2013, **104**, 2686.

30 (*a*) J. D. P. Valentin, X.-H. Qin, C. Fessele, H. Straub, H. C. van der Mei, M. T. Buhmann, K. Maniura-Weber and Q. Ren, *J. Colloid Interface Sci.*, 2019, **552**, 247; (*b*) E. E. Charrier, K. Pogoda, R. G. Wells and P. A. Janmey, *Nat. Commun.*, 2018, **9**, 449.
31 F. Hook, M. Rodahl, B. Kasemo and P. Brzezinski, *Proc. Natl. Acad. Sci. U. S. A.*, 1998, **95**, 12271.
32 (*a*) A. A. Khalili and M. R. Ahmad, *Int. J. Mol. Sci.*, 2015, **16**, 18149; (*b*) W. Huang, B. Anvari, J. H. Torres, R. G. Lebaron and K. A. Athanasiou, *J. Orthop. Res.*, 2003, **21**, 88.
33 M. Lord, C. Modin, M. Foss, M. Duch, A. Simmons, F. Pedersen, B. Milthorpe and F. Besenbacher, *Biomaterials*, 2006, **27**, 4529.
34 B. G. Fox and P. G. Blommel, *Curr. Protoc. Protein Sci.*, 2009, **56**, 5.23.1–5.23.18.